Novel mechanocaloric materials for solid-state cooling applications

Cite as: Appl. Phys. Rev. **6**, 041316 (2019); https://doi.org/10.1063/1.5113620
Submitted: 06 June 2019 . Accepted: 05 December 2019 . Published Online: 26 December 2019

Claudio Cazorla

Applied Physics Reviews REVIEW scitation.org/journal/are

Novel mechanocaloric materials for solid-state cooling applications

Cite as: Appl. Phys. Rev. **6**, 041316 (2019); doi: 10.1063/1.5113620
Submitted: 6 June 2019 · Accepted: 5 December 2019 ·
Published Online: 26 December 2019

Claudio Cazorla[a]

AFFILIATIONS

School of Materials Science and Engineering, UNSW Sydney, Sydney, NSW 2052, Australia

[a]E-mail: c.cazorla@unsw.edu.au

ABSTRACT

Current refrigeration technologies based on compression cycles of greenhouse gases are environmentally threatening and cannot be scaled down to on-chip dimensions. Solid-state cooling is an environmentally friendly and highly scalable technology that may solve most of the problems associated with current refrigerant methods. Solid-state cooling consists of applying external fields (magnetic, electric, and mechanical) on caloric materials, which react thermally as a result of induced phase transformations. From an energy efficiency point of view, mechanocaloric compounds, in which the phase transitions of interest are driven by mechanical stresses, probably represent the most encouraging type of caloric materials. Conventional mechanocaloric materials like shape-memory alloys already display good cooling performances; however, in most cases they also present critical mechanical fatigue and hysteresis problems that limit their applicability. Finding new mechanocaloric materials and mechanisms that are able to overcome those problems, while simultaneously rendering large temperature shifts, is necessary to further advance the field of solid-state cooling. In this article, we review novel families of mechanocaloric materials that in recent years have been shown to be especially promising in the aspects that conventional mechanocaloric materials are not, and that exhibit unconventional but significant caloric effects. We emphasize elastocaloric materials, in which the targeted cooling spans are obtained through uniaxial stresses, since from an applied perspective they appear to be the most accomplished ones. Two different types of mechanocaloric materials emerge as particularly hopeful from our analysis: (1) compounds that exhibit field-induced order-disorder phase transitions involving either ions or molecules (polymers, fast-ion conductors, and plastic crystals), and (2) multiferroics in which the structural parameters are strongly coupled with the polar and/or magnetic degrees of freedom (magnetic alloys and oxide perovskites).

TABLE OF CONTENTS

I. INTRODUCTION

Conventional cooling technologies are based on compression of greenhouse gases that are environmentally threatening (e.g., hydrofluorocarbons). One kilogram of a typical refrigerant gas has the same greenhouse impact as two tons of carbon dioxide, which is the equivalent of running a car uninterruptedly for six months.[1] In addition, current cooling technologies present two other critical drawbacks: (1) the energy efficiency of refrigeration cycles is low (<60%) and (2) their scalability to small dimensions is very limited. Approximately 1.4 billion domestic refrigeration units in the world account for about 15% of the total domestic energy consumption, or equivalently, annual CO_2 emissions of 450×10^6 tons;[2] hence, the potential positive impact on world's sustainability caused by even modest improvements in energy efficiency is enormous. Meanwhile, for microchips to

perform optimally, the heat generated by electric currents needs to be removed from them; therefore, efficient microsized coolers that operate near room temperature are pressingly needed for successfully engineering faster and more compact electronic devices.

Solid-state cooling is an environmentally friendly, highly energy-efficient, and highly scalable technology that may solve most of the problems associated with current refrigerant methods. Solid-state cooling relies on caloric materials and the application of external fields. In caloric materials, reversible temperature shifts are achieved through the application/removal of electric, magnetic, or mechanical fields that render electrocaloric, magnetocaloric, or mechanocaloric (MC) effects, respectively. These caloric effects are originated by field-induced phase transitions that involve large changes in entropy (typically on the order of 10–100 J kg^{-1} K^{-1}). Solid-state cooling energy efficiencies of ∼75% have been demonstrated (although within relatively small temperature spans of ∼1–10 K), and further improvements appear to be within reach.[3] Certainly, the fast response to external stimuli and compactness of caloric materials raise high hopes to surpass the performance, environmental compliance, and portability of current gas-based refrigeration technologies. Caloric materials have actually become a hot topic of research in recent years, as is shown by the rapidly increasing number of related works published in the last decade (Fig. 1).

Elastocaloric (eC) and barocaloric (BC) materials lie in the mechanocaloric (MC) category, for which the driving mechanical fields are uniaxial stress and hydrostatic pressure, respectively [e.g., shape-memory alloys (SMAs)]. Magnetocaloric compounds (e.g., $Gd_5Si_2Ge_2$) are the most well studied of all caloric materials (Fig. 1), and currently they are used in research laboratories for reaching ultra-low temperatures (that is, close to the liquefaction points of nitrogen and helium).[4] The main drawback of magnetocaloric materials is that

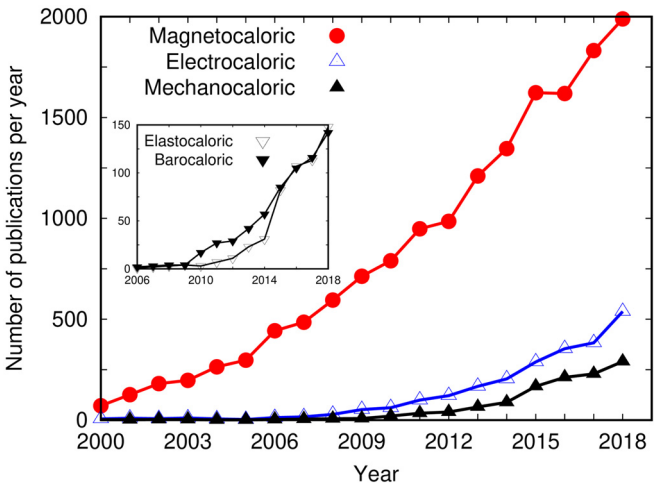

FIG. 1. Number of articles published on caloric materials since 2000 (according to Scopus based searches). The tendency in the three general categories of caloric materials is clearly ascendant, specifically since 2010. The number of publications on magnetocaloric materials is overwhelmingly larger (giant magnetocaloric effects were first reported for Gd-Si-Se alloys in the late 1990s[14]). The number of publications on mechanocaloric materials has increased significantly during the last decade (giant mechanocaloric effects were first reported for shape memory alloys in the early 1980s[15,16]). Inset: the number of publications on elastocaloric and barocaloric materials exhibit a similar increase in the last few years.

they require large magnetic fields to drive normal refrigeration spans and usually contain rare-earth elements that are scarce in nature. Meanwhile, electrocaloric materials (e.g., $PbZr_{0.95}Ti_{0.05}O_3$) are well suited for portable cooling applications owing to their high energy density and natural integration in circuitry.[5–7] However, electrocaloric effects usually are too modest, occur at temperatures different from ambient, and require complex material synthesis processes to minimize impeding leakage currents (even for relatively small electric fields of $\sim 10^1$–10^2 kV/cm).[6]

Elastocaloric materials, on the other hand, present easy and scalable synthesis along with good availability of the constitutive elements, which leads to affordable production costs. Likewise, the large latent heat accompanying the first-order martensitic phase transition in archetypal eC compounds renders excellent cooling performances.[8] Nevertheless, conventional eC materials also present some drawbacks mainly associated with their structural stability, mechanical fatigue, and phase-transition hysteresis, which lead to durability and irreversibility issues that may severely limit their cooling performance and applicability.[9] Finding new MC materials with improved mechanical and phase switching properties is highly desirable for the deployment of sustainable, environmentally friendly, and highly scalable solid-state cooling applications.

In this review article, we survey a large number of MC materials ranging from archetypal shape-memory alloys to less renowned eC compounds like polymers, polar oxides, organometal halide perovskites (OMHPs), molecular crystals, multiferroics (MFs), and fast-ion conductors. Excellent reviews on elastocaloric and barocaloric materials already exist in the literature;[10–13,26] however, the present article, in contrast to those previous ones, focuses on nonconventional MC materials that in recent years have been shown to be particularly promising in the aspects that conventional MC materials are not and that exhibit atypical but sizable MC effects. Our main emphasis is on eC materials since from a technological point of view these are probably the most encouraging; however, we also review novel families of barocaloric materials that exhibit remarkable cooling performances and distinctive field-induced phase transitions. Previous to our eC compounds survey, we present a brief and general description of MC materials and explain the thermodynamics of MC effects and main techniques that are used to measure and predict MC phenomena. The article ends up with a summary of our most relevant conclusions and outlook.

II. SOLID-STATE COOLING

A. Elastocaloric materials: An overview

Elastocaloric materials undergo reversible changes in temperature when uniaxial mechanical stresses are applied on them under adiabatic conditions (that is, when heat transfers with the surroundings are absent). The archetypal class of elastocaloric (eC) effects are those associated with the superelasticity of shape memory alloys (SMA, e.g., nonmagnetic Ni-Ti and Cu-based alloys). SMAs present a high-temperature high-symmetry phase known as austenite and a low-temperature low-symmetry phase known as martensite; it is possible to move from one phase to another by means of shear strains. Specifically, a SMA in the austenite phase releases heat into the surroundings when it is stressed uniaxially and the martensite phase is stabilized; conversely, the SMA absorbs heat from the surroundings when returning back to the austenite phase upon release of the applied

uniaxial stress. Thermal effects associated with the strain-driven austenite-martensite phase transition have been known for about 40 years;[15,16] however, it has not been until recently that eC effects have been recognized as a potential strategy for room-temperature cooling.[17,133]

Ideal eC materials should render large adiabatic temperature spans, ΔT ($\sim$10 K), under the application of small or moderate uniaxial stresses (typically 10^2–10^3 MPa) at (or near) room temperature. We note that the amount of heat that a caloric device can exchange with a hot/cold source is an extensive variable, that is, it scales with the amount of caloric material that is contained in it. This condition imposes a number of device engineering challenges. For instance, a thin film exhibiting a giant adiabatic temperature shift may be very useful as an on-chip cooler but it may be not able to refrigerate an entire lap-top computer. Therefore, ΔT may not necessarily be the most important parameter defining a "good" mechanocaloric material.

A parameter that quantifies the cooling performance of eC materials is the cooling/heat pumping cycle efficiency (COP), which is defined as

$$COP = \frac{|Q|}{W} = \frac{m \cdot c \cdot |\Delta T|}{\frac{1}{\rho}\oint \sigma \cdot d\varepsilon}, \tag{1}$$

where $|Q|$ and W represent the amount of exchanged heat and mechanical work done on the material, respectively, m is the molar mass, c is the molar heat capacity, ρ is the density, and σ and ε are the applied uniaxial stress and resulting uniaxial strain, respectively. Typical COP values of efficient eC materials lie within the range of 2–8.[18]

Another useful refrigerant performance descriptor is the so-called refrigerant capacity (RC), which is defined as

$$RC = \int_{T_0}^{T_1} \Delta S \cdot dT, \tag{2}$$

where T_0 and T_1 represent the lower and upper temperatures delimiting the interval in which the caloric effects of interest are observed. Likewise, one can define the normalized refrigerant capacity (NRC) which corresponds to the RC divided by the applied external field variation, ΔX ($\Delta\sigma$ in the case of eC effects)

$$NRC = \frac{RC}{\Delta X}. \tag{3}$$

Typical RC and NRC values of good MC materials are on the order of 1 kJ kg^{-1} (5 J cm^{-3}) and 10 kJ kg^{-1} GPa^{-1}, respectively.[10,19]

A number of prototypes based on eC materials already exist, which are mostly based on Ni-Ti SMA (for a detailed description of such prototypes see Ref. 20). Typical values of device COP (which normally are lower than the corresponding material COP—Eq. (1)—due to irreversible heat transfer losses that occur in practice) and pumping power are around unity and $\sim$10 W, respectively. Such prototypes can be classified into two broad categories depending on the method used for transferring heat from the cool to the heat source. The first class of prototypes refers to devices in which the eC compound remains stationary and a fluid is circulated to facilitate heat transfer.[21,22] In the second category, the eC element is mobile and heat transfer is realized by direct contact with the cool and heat sources.[23]

Active elastocaloric refrigerators (i.e., involving heat exchangers, eC plates, a heat-transfer fluid, and an actuator to load/unload the material) have been already designed,[24] and a regenerative eC device has been recently shown to exceed the performance of previous refrigerant devices based on the magnetocaloric effect.[25] Although there are still few technical aspects that need to be improved (e.g., cyclability, materials fatigue, and heat transfer), such prototypes illustrate very well the great potential of elastocaloric materials in the context of solid-state cooling.

B. The elastocaloric effect

When uniaxially stressed, eC materials undergo a change in temperature under adiabatic conditions, ΔT, or equivalently a change in entropy under isothermal conditions, ΔS. The entropy of a system subject to an external uniaxial stress, σ, depends on the applied load and temperature, T; hence, an infinitesimal change in entropy can be expressed as

$$dS = \left(\frac{\partial S}{\partial \sigma}\right)_T d\sigma + \left(\frac{\partial S}{\partial T}\right)_\sigma dT. \tag{4}$$

The partial derivative of the system entropy with respect to temperature is related to the heat capacity, C (at fixed stress), as

$$\left(\frac{\partial S}{\partial T}\right)_\sigma = \frac{C}{T}. \tag{5}$$

Likewise, the Maxwell relation,

$$\left(\frac{\partial S}{\partial \sigma}\right)_T = V_0\left(\frac{\partial \varepsilon}{\partial T}\right)_\sigma, \tag{6}$$

allows us to express the stress derivative of the system entropy as a function of its T-induced elongation, ε, at fixed uniaxial stress (V_0 corresponds to the equilibrium system volume). By considering the thermodynamic relations (5) and (6), one can rewrite dS in a physically more insightful manner such as

$$dS = V_0\left(\frac{\partial \varepsilon}{\partial T}\right)_\sigma d\sigma + \frac{C}{T}dT. \tag{7}$$

From Eq. (7), it is straightforward to deduce the analytical expression of the entropy change that an eC material experiences upon application of uniaxial stresses at fixed temperature (that is, $dT = 0$), namely,

$$\Delta S = V_0 \int_0^\sigma \left(\frac{\partial \varepsilon}{\partial T}\right)_{\sigma'} d\sigma', \tag{8}$$

as well as the expression of the corresponding temperature change occurring under adiabatic conditions (that is, $dS = 0$), which is

$$\Delta T = -V_0 \int_0^\sigma \frac{T}{C}\left(\frac{\partial \varepsilon}{\partial T}\right)_{\sigma'} d\sigma'. \tag{9}$$

When temperature changes are small and the heat capacity of the system does not change appreciably in the considered σ interval, the adiabatic temperature change of an eC material can be reasonably approximated by

$$\Delta T \approx -\frac{T}{C}\Delta S. \tag{10}$$

The equation above shows that a negative isothermal entropy shift leads to a positive adiabatic temperature shift (heating, conventional

eC effect), and conversely, a positive ΔS leads to a negative ΔT (cooling, inverse eC effect). Elastocaloric effects associated with SMAs normally are conventional during stress loading. When the phase transition rendering eC effects is of first-order type, one can use the Clausius-Clapeyron method to express the accompanying isothermal entropy change as[26]

$$\Delta S = -V_0 \, \Delta\varepsilon \, \frac{d\sigma}{dT}, \tag{11}$$

where $\Delta\varepsilon$ represents the change in length that the material experiences during the transformation along the direction of the applied stress, and the derivative the T-induced variation of the critical stress field required to induce the transformation. We note that the Clausius-Clapeyron method disregards possible caloric effects in each of the involved phases at thermodynamic conditions other than the transition point, which usually are small.[26]

A simple four-step cooling cycle based on eC materials (and in general on any caloric compound) can be envisaged which consists of two adiabatic and two nonisothermal processes (Fig. 2). Starting from the high-symmetry high-T phase at temperature T_1, a uniaxial stress is applied adiabatically on the sample that stabilizes the corresponding low-symmetry low-T phase. Consequently, the temperature of the eC element increases up to $T_2 = T_1 + \Delta T$, where the size and sign of ΔT depend on the material and applied stress [Eq. (9)]. The eC material, which still remains elastically strained, is then put into contact with a thermal sink so that heat is ejected from the system. Consequently, the temperature of the eC element returns back to T_1 and its entropy becomes smaller than it was at the beginning of the cycle. Subsequently, the uniaxial stress is adiabatically removed and the temperature of the eC element falls down to $T_4 = T_1 - \Delta T$. Finally, the eC component is put into contact with the hot source that needs to be cooled down so that the heat is absorbed by the system and the initial values of the temperature and entropy are restored.

C. Experimental and theoretical measurement techniques

In practice, the temperature and entropy increments associated with eC effects are measured with direct or indirect methods. Direct methods refer to *in situ* temperature measurements on the samples

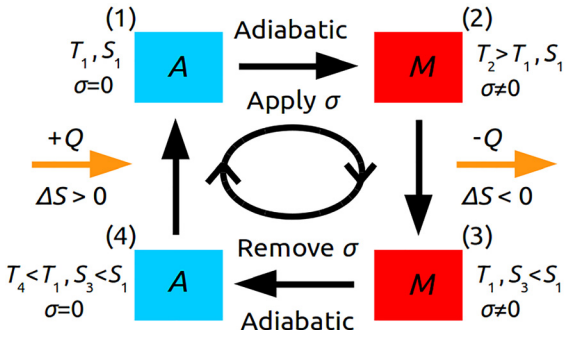

FIG. 2. Sketch of the typical four-step refrigerant cycle based on eC materials (see main text). "A" stands for the initial high-symmetry high-T phase of the system in the absence of any stress (e.g., austenite phase in SMA) and "M" for the corresponding strain-induced low-symmetry low-T phase (e.g., martensite phase in SMA).

during the stress loading/unloading cycles. Indirect methods, on the other hand, involve strain measurements under varying uniaxial stress and temperature conditions that allow us to estimate ΔT and ΔS through the Maxwell relations [for instance, Eq. (8)]. When the phase transition rendering eC effects is of first-order type, one may use the Clausius-Clapeyron method [for instance, Eq. (11)]; this is a particular case of indirect methods that involve the determination of transition temperatures during cooling and heating cycles.

Direct methods (e.g., thermocouples mounted on the samples and thermography IR cameras) are more straightforward than indirect methods; however, they are also more prone to be affected by systematic errors (actually, caloric data obtained with direct and indirect methods normally differ[27]). For instance, since the eC material needs to be connected to an actuator-like element for stress loading and unloading, in practice there will always be heat leakages to the ambient that will lead to irreversible processes (i.e., nonadiabaticity) and consequently to underestimation of ΔS. There is a third category of measurement techniques, namely quasidirect methods, which employs differential scanning calorimetry to measure directly heat transfers, which can be converted subsequently into entropy and temperature changes. This last type of technique is particularly well suited for barocaloric measurements but entails some technical challenges when it comes to measuring elastocaloric effects.

A different way of estimating eC effects is with theoretical methods. Theoretical methods are inexpensive from an economical cost point of view, can be very accurate, and have predictive power; hence, they may serve as a guide for the experiments. By theoretical methods we refer to first-principles methods (e.g., density functional theory[28,29]), atomistic simulation techniques (,e.g., classical molecular dynamics and Monte Carlo methods—see, for instance, Ref. 30), and phenomenological and effective Hamiltonian models (see, for instance, Refs. 24 and 31). A particularly promising computational technique that allows us to estimate phase-transition entropies and heat capacities in crystals is the quasiharmonic (QH) approach.[32,33] In the QH approach, one first computes the vibrational frequencies of a material, $\omega_{\boldsymbol{q}s}$ (for instance, with the "small displacement" method[34,35]) and subsequently obtains the corresponding lattice entropy, S_{latt}, and heat capacity, C_{latt}, through the exact analytical expressions

$$S_{latt}(T) = -\frac{1}{N_{\boldsymbol{q}}} k_B \sum_{\boldsymbol{q},s} \ln\left[2\sinh\left(\frac{\hbar\omega_{\boldsymbol{q}s}}{2k_B T}\right)\right], \tag{12}$$

$$C_{latt}(T) = \frac{1}{N_{\boldsymbol{q}}} \sum_{\boldsymbol{q},s} \frac{(\hbar\omega_{\boldsymbol{q}s})^2}{k_B T^2} \cdot \frac{e^{\frac{\hbar\omega_{\boldsymbol{q}s}}{k_B T}}}{\left(e^{\frac{\hbar\omega_{\boldsymbol{q}s}}{k_B T}} - 1\right)^2}, \tag{13}$$

where $N_{\boldsymbol{q}}$ is the total number of wave vectors used for integration within the Brillouin zone and the summation runs over all wave vectors $\boldsymbol{q}$ and phonon branches s. The main disadvantage of the QH approach is that strong anharmonic effects are completely disregarded; hence, one needs to check explicitly in each case whether or not this approximation compromises the reliability of the obtained theoretical results.[36–38] In addition, possible sources of entropy other than lattice vibrations need to be considered separately (e.g., stemming from the magnetic and electronic degrees of freedom).[7,39]

Other less conventional types of computational approaches (for instance, based on high-throughput searches, which are becoming increasingly more popular within the community of materials scientists)

have been employed also recently for the design of new caloric materials.[40,41] A detailed description of the above-mentioned theoretical methods escapes from the scope of the present review, but we will refer to the relevant works when necessary.

It should be noted that caloric effects predicted or estimated with computational and simulation methods tend to be larger in magnitude than those measured in practice (see Secs. IV and V). Possible sources of errors in the theoretical models include (1) simplifications made in the adopted structural models (e.g., simulated systems typically are surface/interface free and do not contain crystallographic defects), (2) simplifications made in the account of the interatomic interactions (e.g., the force fields employed in classical molecular dynamics may be of limited accuracy and not always adequate for reproducing finite-stress conditions), and (3) neglection of possible sources of entropy other than the primary ones (e.g., the couplings between different order parameters may lead to sizable secondary caloric effects, which typically are disregarded). In addition, relatively large driving stresses that in practice cannot be applied to real samples (i.e., they are larger than the experimental failure stresses) typically are considered in the simulations.

For the above reasons, although experimental studies are neither free of technical complexities nor of accuracy issues,[27] it is very desirable to validate in the laboratory those theoretical predictions that are of potential relevance to the community of researchers working on caloric effects and materials. In this sense, accurate and reliable simulation/computational studies in general represent a very valuable guidance and motivation to experimentally focused studies and research groups.

III. ARCHETYPAL eC MATERIALS: SHAPE-MEMORY ALLOYS

Shape-memory alloys (SMAs) are archetypal ferroelastic materials in which the lattice distortions are dominated by shear strains. Generally, SMAs possess very good ductility: they can be strained by about 10% and more. These superb elastic properties along with the large latent heat associated with the austenite to martensite phase transition ($|\Delta S| \sim 10\,\mathrm{J\,kg^{-1}\,K^{-1}}$) convert SMAs into excellent eC materials. SMAs can be divided into two broad groups, namely, magnetic (e.g., Ni-Mn-Sb-Co and Ni-Fe-Ga alloys) and nonmagnetic (e.g., Ni-Ti based, Cu-based, and Fe-based alloys). The most widely investigated class of eC materials are near-equiatomic Ni-Ti alloys (Table I). The high-temperature phase of Ni-Ti alloys, usually denoted as austenite, presents cubic symmetry (Fig. 3) and is easily deformable by shearing the {110} planes along the ⟨1–10⟩ direction. The phonon branch associated with such a distortion (labelled as TA_2) and the corresponding elastic constant (C') are both "soft," thus leading to high vibrational entropy and the stabilization of the austenite phase at high temperatures.[42] The austenite-martensite phase transition is diffusionless and of first-order type. The low-temperature martensite phase in Ni-Ti alloys is monoclinic (space group $P21/m$, Fig. 3), although other intermediate crystal structures may be observed in the experiments depending on the chosen heat treatment and chemical composition of the material samples.

In Table I, we summarize the properties of some SMA-based compounds in which giant eC effects (i.e., $|\Delta S| \sim 10\,\mathrm{J\,kg^{-1}\,K^{-1}}$ and $|\Delta T| \sim 10\,\mathrm{K}$) have been observed. For instance, an adiabatic temperature change of 25 K (21–17 K) under application (removal) of a ∼500 MPa stress tension has been measured in Ni-Ti wires.[43,44] Likewise, a $|\Delta T|$ of 17 K (16 K) under stress loading (unloading) has been observed in a Ni-Ti thin film.[45] Very recently, a colossal elastocaloric adiabatic temperature change of 31.5 K has been measured in NiMn-based bulk polycrystalline alloys ($|\Delta S| = 45\,\mathrm{J\,kg^{-1}\,K^{-1}}$) for a uniaxial load of 700 MPa at near room temperature conditions ($T = 308\,\mathrm{K}$).[130]

TABLE I. SMA in which giant eC effects have been experimentally observed. T_t represents operating temperature, C heat capacity, ε uniaxial strain, $\Delta\sigma$ applied uniaxial stress, ΔS_t entropy change associated with the phase transition, ΔT_t adiabatic temperature change deduced from the entropy change associated with the phase transition, and $\Delta T_{(d)}$ adiabatic temperature change that is measured directly. (w) stands for wire and (f) for thin film.

Compound	C ($\mathrm{J\,kg^{-1}\,K^{-1}}$)	T_t (K)	$\lvert\varepsilon\rvert$ (%)	$\lvert\Delta S_t\rvert$ ($\mathrm{J\,kg^{-1}\,K^{-1}}$)	$\lvert\Delta T_t\rvert$ (K)	$\lvert\Delta T_{(d)}\rvert$ (K)	$\lvert\Delta\sigma\rvert$ (MPa)	References
$Ni_{50}Ti_{50}$ (w)	550	300	8	40	22	25	500	43
$Ni_{50}Ti_{50}$ (f)	420	260	3.5	77	48	16	500	45
$Ni_{45}Ti_{47}Cu_5V_3$	500	250	5	40	20	8	500	54
$Ni_{31}Ti_{55}Cu_{12}Co_2$	420	280	2	30	20	10	200	49
$Ni_{54}Fe_{19}Ga_{27}$	470	280	3	11	6	4	170	55
$Ni_{54}Fe_{19}Ga_{27}Co_4$	450	300	5	11	7	10	300	56
$Ni_{33}Co_{40}Al_{29}$	480	290	10	44	26	3	50	47
$Ni_{43}Mn_{40}Sn_{10}Cu_7$	450	320	1	54	38	…	10	57
$Ni_{46}Mn_{38}Sb_{12}Co_4$	400	300	3	34	25	…	100	58
$Ni_{45}Mn_{44}Sn_{11}$	580	270	2	32	15	6	260	59
$Ni_{45}Mn_{36}In_{14}Co_5$	460	250	3	18	10	4	150	60
$Ni_{48}Mn_{35}In_{17}$	400	300	2	40	30	4	250	61
$Cu_{68}Zn_{16}Al_{16}$	430	230	8	21	22	6	120	17, 50
$Cu_{83}Al_{14}Ni_3$	410	250	8	21	13	16	150	15
$Fe_{49}Rh_{51}$	470	310	0.3	13	8	5	500	52
$Fe_{69}Pd_{31}$	400	250	2	1	0.6	3	200	53
$(Ni_{50}Mn_{31.5}Ti_{18.5})_{99.8}B_{0.2}$	470	308	7	45	31.5	31.5	700	130

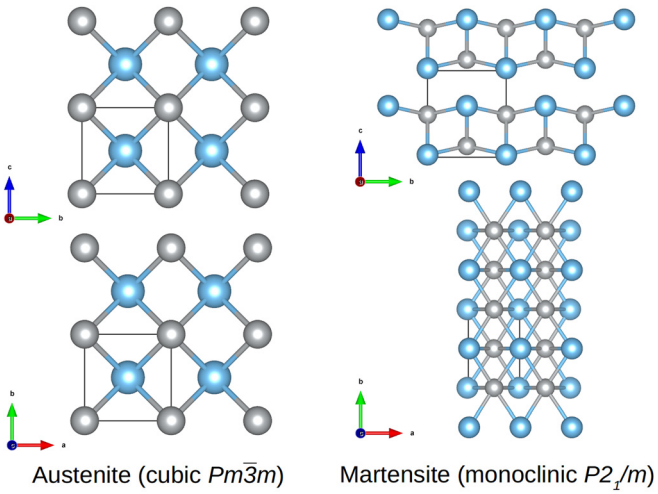

FIG. 3. Ball-stick representation of the usual high-temperature high-symmetry austenite and low-temperature low-symmetry martensite phase in Ni-Ti based alloys. Ni and Ti atoms are represented by gray and blue spheres, respectively. The unit cell dimensions in each phase are indicated with thick black lines.

SMA alloys present two main drawbacks in the context of eC cooling.[9,10] One is related to the unavoidable hysteresis effects associated with the first-order nature of the martensitic phase transition. Hysteresis originates from the fact that the transition path occurs under nonequilibrium conditions; hence, irreversible processes take place within the material. From a practical point of view, irreversibility may pose severe limitations to the overall cooling performance attained during successive field-induced cycles. In particular, the irreversibility of any caloric effect depends on two parameters:[10] (1) the temperature width of the hysteresis and (2) the temperature-shift of the entire hysteresis loop due to the application/removal of the external field (Fig. 4). Certainly, the narrower the hysteresis, the smaller is the irreversibility of the process. On the other hand, if the width of the hysteresis is significant, a large temperature shift of the characteristic transition temperature as induced by the application of the external field may lead to a considerable reduction in irreversibility (Fig. 4).

Recently, it has been shown in magnetic SMA that a possible way of improving the reversibility of cooling effects is to exploit hysteresis effects in thermodynamic cycles that combine different types of external stimulus (e. g., magnetic and mechanical);[46] we will comment again in this case later on when reviewing "multicaloric" materials. Last but not least, a remarkable fully reversible adiabatic temperature shift of 31.5 K has been measured very recently in the magnetic SMA $(Ni_{50}Mn_{31.5}Ti_{18.5})_{99.8}B_{0.2}$ near room temperature.[130] This latter experimental study shows that chemical strategies could be used to mostly overcome the reversibility issues found in archetypal elastocaloric materials.

Another non-negligible drawback of SMA alloys is related to their mechanical stability and fatigue. This family of materials displays two different types of fatigue: (1) structural fatigue, as originated by conventional cracks formation and propagation eventually leading to fracture, and (2) functional fatigue, linked to the loss of superelastic properties over the increasing number of cycles. These issues typically limit the durability of SMA alloys to just few thousands of cycles, which is insufficient for practical applications (e.g., heat-pumping devices).

Aimed at improving the structural stability and mechanical fatigue properties of Ni-Ti alloys, doping strategies based on Cu, Co, Fe, and V have been explored. In Ni-Fe-Ga and Ni-Co-Al alloys, for instance, adiabatic temperature spans of 8.4 and 3.1 K have been measured directly, while values about a factor of 2 larger have been estimated indirectly.[47] An adiabatic temperature change of 10 K has been observed in Ni-Ti-Cu-Co thin films, which remarkably can endure several millions of loading-unloading strain cycles of $|\varepsilon| \sim 2.5\%$.[48,49] Among Cu-based SMA, Cu-Zn-Al has received special attention; a $|\Delta T|$ of 15 K has been measured indirectly for a small uniaxial stress of 28.5 MPa.[17,50,51] A negative adiabatic temperature shift of 6 K (i.e., inverse eC effect) has been also observed in Cu-Zn-Al alloys at temperatures below ambient. Among Fe-based SMA, Fe-Rh and Fe-Pd alloys have been found to display large and giant eC effects; adiabatic temperature changes of 5–8 K have been reported in Fe-Rh near room

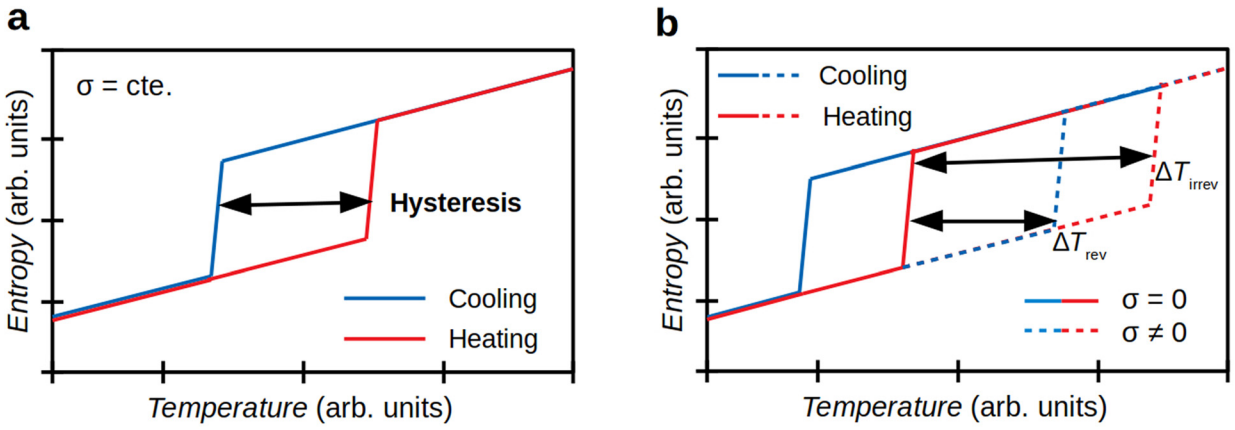

FIG. 4. Sketch of hysteresis and irreversibility effects in elastocaloric materials undergoing a phase transition (identified by an abrupt change in entropy). (a) Hysteresis is manifested as a phase transition temperature lag between the cooling and heating processes. (b) Reversible adiabatic temperature changes, ΔT_{rev}, can be estimated by considering the heating (or cooling) process under null stress ($\sigma = 0$) and the cooling (or heating) process under finite stress ($\sigma \neq 0$). Considering only the heating or cooling processes in both the null and finite stress cycles typically leads to an overestimation of the reversible adiabatic temperature shift, ΔT_{irrev}.

temperature[52] and of 2 K in Fe-Pd under moderate uniaxial stresses (~500 MPa).[53]

Likewise, large eC effects have been observed in magnetic SMAs such as Ni-Fe-Ga[55,56] and Ni-Mn-Sb-Co[57,58] alloys near room temperature. For instance, an adiabatic temperature change of 10 K has been measured directly in $Ni_{54}Fe_{19}Ga_{27}Co_4$ at $T = 300$ K and $|\Delta\sigma| = 300$ MPa.[56] Nevertheless, magnetic SMA alloys, in contrast to nonmagnetic SMAs, typically are brittle[131] and consequently cannot withstand large uniaxial deformations.

As regards possible cooling applications, the temperature span over which large ΔS and ΔT are observed should be as large as possible. The refrigerant cooling performance (RCP), defined as $RCP = |\Delta S_{peak}| \times |\text{FWHM of } \Delta S(T)|$ where "FWHM" stands for full width at half maximum [hence, it has units of temperature, see Eq. (2)], is a good indicator of such a quality. In a recent study,[51] an outstanding RCP of 2300 J kg^{-1} has been measured in a Cu-Zn-Al polycrystal, which in fact demonstrates the great promise of SMA for realizing practical mechanocooling devices.

IV. NONCONVENTIONAL eC MATERIALS

In the last few years, families of materials other than SMAs have been reported to exhibit also large or giant eC effects (Table II). Examples include organic-inorganic polymers,[62–64] polar materials,[65–69] fast-ion conductors,[70–72] hybrid perovskites,[73] and multiferroics.[46] Although SMAs may outperform such nonconventional eC materials in some facets, the latter present huge room for improvement since they have not been yet optimized or fully analyzed and are particularly promising in the aspects that SMAs are not (e.g., large $|\Delta T|$'s, high mechanical stability, and low hysteresis). In this section, we explain and summarize the properties of nonconventional eC compounds (which have not been considered in detail in previous review articles) in an attempt to broaden the scope of mechanocaloric materials and of solid-state cooling in general.

A. Hybrid organic-inorganic polymers

Natural rubber was the first material in which elastocaloric effects were observed.[74] Recently, the eC properties of this material have been revisited. Natural rubber is an elastomer consisting of randomly oriented polymeric chains. Upon application of uniaxial stress, the polymeric chains in natural rubber become ordered along the direction of the strain, which produces a decrease in the configurational entropy of the system (hence the origin of the observed eC effect). Adiabatic temperature changes of 9–12 K have been measured directly in natural rubber near room temperature for huge uniaxial strains of ~600% (resulting from minute uniaxial stresses of just 1–2 MPa).[62,75]

Polymers based on polyvinylidene fluoride (PVDF) also conform to a promising family of eC materials. These polymers are ferroelectrics, that is, they exhibit spontaneous and switchable electric polarization, and the accompanying polar to nonpolar phase transition is very sensitive to external mechanical stresses (hence the origin of the reported eC effects). Giant electrocaloric effects have also been reported recently in these materials.[76] Adiabatic temperature changes of ~2 K have been measured directly in PVDF polymers near room temperature under moderate uniaxial strains of ~10% (equivalent to small uniaxial stresses of ~10 MPa). The reported adiabatic temperature changes in PVDF polymers normally are large but not giant in particular due to the huge heat capacity of such light-weight materials [i.e., $C \sim 1700$ JK^{-1} kg^{-1} (Ref. 76) to be compared with typical SMA values of ~500 JK^{-1} kg^{-1}, Table I].

TABLE II. Materials other than SMAs in which large eC effects have been experimentally observed or predicted with theory/simulation methods. T_t represents operating temperature, ε uniaxial strain, $\Delta\sigma$ applied uniaxial stress, ΔS_t entropy change associated with the phase transition, and ΔT_t adiabatic temperature change deduced from the entropy change associated with the phase transition. (f) stands for thin film, PVDF for polyvinylidene di-fluoride polymers, "VNR" for vulcanized natural rubber, and "PDMS" for polydimethylsiloxane. "POL," "FE," "AFE," "FIC," "HP," and "MF" indicate organic-inorganic polymers, polar materials, antiferroelectric, fast-ion conductors, hybrid perovskites, and multiferroic, respectively. "E" and "T" in the reference column indicate whether the work is experimental or theoretical, respectively.

Compound	Material type	T_t (K)	$\lvert\varepsilon\rvert$ (%)	$\lvert\Delta S_t\rvert$ (J kg^{-1} K^{-1})	$\lvert\Delta T_t\rvert$ (K)	$\lvert\Delta\sigma\rvert$ (MPa)	References
Natural rubber	POL	300	600	80	9–12	1–2	62, 75 *E*
PVDF	POL	300	12	11	2	15	63, 64 *E*
VNR	POL	300	6	87	10	173	77 *E*
PDMS	POL	300	6	70	12	173	78 *E*
BCZTO	FE	340	0.2	…	2	250	67 *E*
$BaTiO_3$	FE	300	3	8	5	6500	65, 66 *T*
$Ba_{0.5}Sr_{0.5}TiO_3$	FE	260	1.2	…	9	1000	31 *T*
$PbTiO_3$	FE/MF	700	1.5	…	35	1000	79 *T*
$PbZrO_3$	AFE/MF	950	0.8	…	25	2000	80 *T*
CaF_2 (f)	FIC	1350	2.8	200	163	5000	70 *T*
PbF_2 (f)	FIC	600	0.5	60	22	600	70 *T*
AgI (f)	FIC	300	10	30	38	1000	71 *T*
$LiIO_3$ (f)	FIC	1000	2	16	9	1000	71 *T*
Li_3N	FIC	300	2	20	2	5800	72 *T*
$CH_3NH_3PbI_3$	HP	300	1	…	11	550	73 *T*
$Ni_{49.6}Mn_{35.6}In_{14.8}$	MF	293	3.5	…	1.3	75	46 *E*
$FeRh/BaTiO_3$	MF	390	…	8	5.2	…	113 *E*

More recently, large elastocaloric effects around room temperature have been reported for vulcanized natural rubber (VNR)[77] and polydimethylsiloxane (PDMS).[78] One advantage of elastomers is that they exhibit giant eC effects around room temperature even in the absence of conventional structural phase transitions. Consequently, the degree of reversibility associated with such eC effects is very high and hysteresis and phase coexistence issues should be practically absent in cooling cycles employing them. It should be noted that the authors of Refs. 77 and 78 classified the caloric effects measured in elastomer samples as "barocaloric" (that is, produced by hydrostatic pressure). However, based on the facts that (1) a pressure-transmitting medium was absent in their experimental setups, (2) the applied mechanical stresses were highly directional, and (3) Eqs. (8)–(9) were employed to estimate indirectly ΔT and ΔS, we have tentatively classified them here as "elastocaloric."

B. Ferroelectric oxide perovskites

Ferroelectric (FE) oxide perovskites are piezoelectric materials. Piezoelectricity is the quality by which an electrical current can be created in a material through the application of a mechanical stress and vice versa. Ferroelectric oxide perovskites generally are very sensitive to strains.[81] In addition, FE oxide perovskites may endure large mechanical deformations when finely synthesized as thin films (e.g., a huge and reversible strain of 14% driven either by an electric field or temperature has been experimentally observed in epitaxially strained multiferroic $BiFeO_3$[82]). Moreover, polar to nonpolar phase transitions occurring in FE oxide perovskites typically are soft-mode driven and of second-order (or weak first-order) type; consequently, accompanying hysteresis effects leading to irreversibility and mechanical fatigue issues may turn out to be relatively small.

The archetypal FE oxide perovskite is $BaTiO_3$ (BTO), which at low temperatures presents a rhombohedral phase characterized by an electric polarization oriented along the pseudocubic direction[111] (Fig. 5). As temperature is increased, BTO undergoes a series of abrupt electrostructural phase transformations: first from the rhombohedral (R) ground state to an orthorhombic (O) phase ($T_t = 180$ K), with the electric polarization along [110], subsequently to a tetragonal (T) phase ($T_t = 280$ K), with the electric polarization along [001], and finally to a nonpolar cubic (C) phase ($T_t = 400$ K)[83] (Fig. 5). Such a sequence of T-induced phase transformations, or sections of it, is observed in many other functional materials, including perovskite-structured compounds (e.g., $CH_3NH_3PbI_3$[84]) and ferroelectric relaxors (e.g., $(Na_{0.5}Bi_{0.5})_{1-x}Ba_xTiO_3$[85]). Interestingly, the R-O-T-C phase transition sequence can also be induced through mechanical stresses at fixed temperature.[28,86] The significant changes in electrical polarization and structural parameters occurring during such phase transitions lie at the heart of most caloric effects observed in FE oxide perovskites.

Small eC effects have been predicted with theory for $BaTiO_3$ at room temperature, in particular, $|\Delta T| \sim 5$ K for huge uniaxial stresses of several thousands of megapascals (Table II).[65,66] A similar adiabatic temperature change has been measured in a related oxide compound, namely $(Ba_{0.85}Ca_{0.15})(Zr_{0.1}Ti_{0.9})O_3$, although in this case it has been for a significantly smaller uniaxial stress ($\sigma \sim 250$ MPa).[67] Of particular promise are the eC effects predicted with simulation methods in $Ba_{0.5}Sr_{0.5}TiO_3$ near room temperature, i.e., $|\Delta T| \sim 10$ K, since these are partly originated by the strong coupling between the elastic and polar degrees of freedom in the material, a common trait in many ferroelectric perovskites.[31]

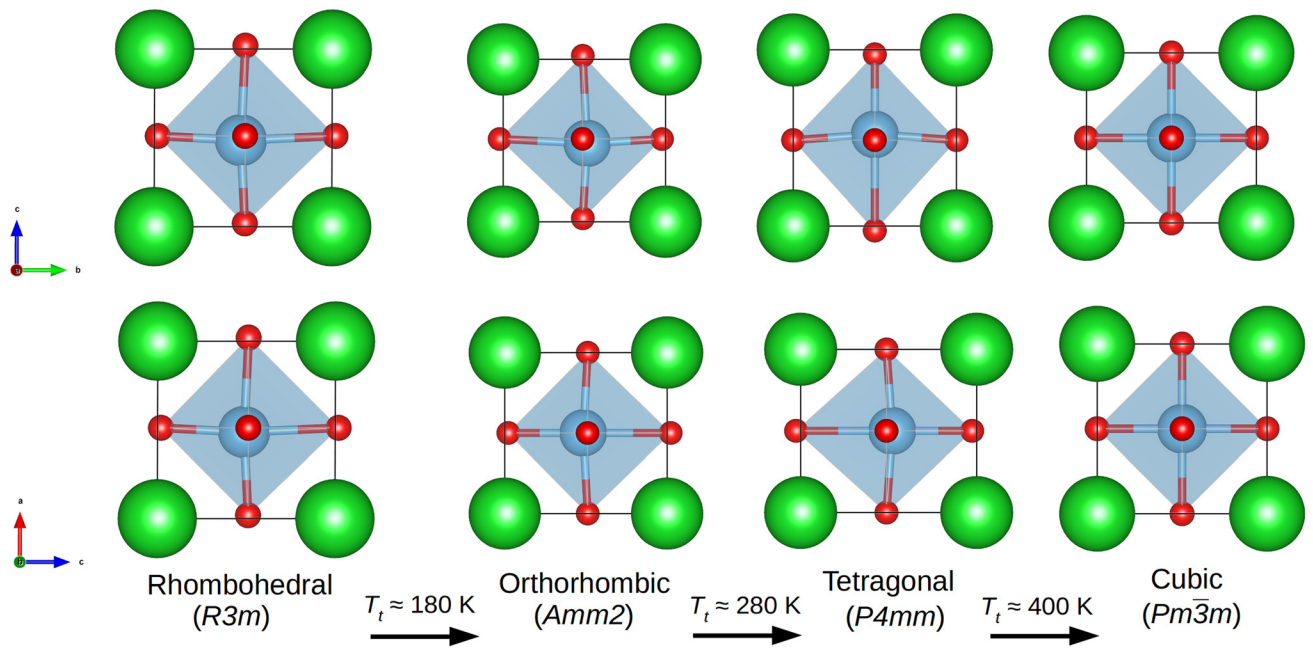

FIG. 5. Representation of the phase transition sequence occurring in the archetypal ferroelectric compound $BaTiO_3$ under increasing temperature. Ba, Ti, and O atoms are represented with green, blue, and red spheres, respectively. The rhombohedral, orthorhombic, and tetragonal phases are polar, whereas the cubic phase is nonpolar (i.e., centrosymmetric). The space group of each relevant phase is indicated within parentheses along with the involved transition temperatures.

Exploitation of the coupling between several ferroic orders that coexist in a same compound (e.g., elastic, electric, and magnetic), usually referred to as multiferroicity, in fact has been suggested as a possible route for achieving giant caloric effects.[87] In this context, a giant adiabatic temperature change of ∼35 K has been predicted in the well-known ferroelectric material $PbTiO_3$ (PTO), which has been ascribed to the mixed ferroelastic and ferroelectric behaviors exhibited by this compound.[79] Unfortunately, in this latter case the transition temperature at which the giant eC effects occur is too high (∼700 K, although large room-temperature eC effects have also been predicted for PTO polycrystals[88]) and the material in question contains toxic elements (i.e., Pb). For completion purposes, we report in Table II the eC effects that have been predicted theoretically for the antiferroelectric compound $PbZrO_3$,[80] which are originated by very similar physical mechanisms to those found in PTO.

C. Fast-ion conductors

Fast-ion conductors (FICs) are materials that exhibit very high ionic conductivity in the crystal phase at temperatures well below their corresponding fusion points.[89] Examples of FICs, which are also known as superionic conductors, include metal fluorides (e.g., CaF_2 and PbF_2), metal iodides (e.g., AgI), oxides (doped CeO_2), metal chalcogenides (e.g., Cu_2Se and Ag_2S), and lithium-based (e.g., Li_3N and $Li_{10}GeP_2S_{12}$) compounds. Currently, FICs are being investigated very intensively in the field of electrochemical devices since these materials are employed as electrolytes in solid-state batteries.

The normal to superionic phase transition in a FIC is associated with a very large change of entropy (∼100–200 $JK^{-1}\,kg^{-1}$) and can be modulated by external fields.[90,91] In particular, the application of mechanical stresses has been proved as an effective means to significantly lower or raise the superionic transition temperature in several archetypal FICs.[92] The physical causes for these effects are the σ-induced lowering or increase in the kinetic energy barriers and formation energy of defects (e.g., Frenkel pairs) that intervene on ionic migration (Fig. 6).[92] Importantly, changes in the ionic conductivity typically are accompanied by large variations in the crystal lattice and volume.[89] Tuning of the ionic conductivity in superionic materials by means of mechanical stresses, and hence of their entropy, presents great prospects in the context of mechanocaloric solid-state cooling (Table II).

FICs can be broadly classified into type-II and type-I categories, depending on whether the normal to superionic phase transition occurs in a continuous (type-II) or abrupt manner (type-I). CaF_2 is an archetypal type-II FIC with the cubic fluorite structure and a very high superionic transition temperature of ∼1350 K.[89] Giant eC effects of $|\Delta S| = 200\,J\,kg^{-1}\,K^{-1}$ and $|\Delta T| = 163$ K have been predicted in CaF_2 thin films under large tensile loads of ∼5000 MPa by means of atomistic-based simulation methods.[70] Despite that these theoretical findings in principle are of little practical relevance due to the high operation temperature involved, they come to show the great mechanocaloric potential that other similar materials with significantly lower superionic transition temperatures may present. This is the case, for instance, of PbF_2 and Li_3N, in which giant adiabatic temperature changes of 22 and 2 K have been predicted to occur at 600 K (Ref. 70) and room temperature,[72] respectively.

Similarly, giant room-temperature eC effects of $|\Delta S| = 30\,J\,kg^{-1}\,K^{-1}$ and $|\Delta T| = 38$ K have been predicted in AgI thin films (a prototype type-I FIC) under moderate compressive stresses of ∼1000 MPa.[71] In this case, the mechanocaloric effects are originated by a σ-induced diffusionless order-disorder phase transition.[71,92] It should be noted that giant mechanocaloric effects induced by hydrostatic pressure have been measured in practice in bulk AgI above room temperature by means of quasidirect methods based on differential scanning calorimetry[120] (Sec. V). Such theory-motivated experimental outcomes illustrate the usefulness of atomistic simulation works when it comes to identify novel families of caloric materials.

A remarkable feature of type-II FICs (for instance, Li_3N) is that possible refrigeration cycles based on them in principle should not suffer from the usual mechanical hysteresis issues affecting other families of eC materials (e.g., shape-memory alloys) since the normal to superionic phase transition is of second-order type and does not involve the nucleation of order-parameter domains or coexistence of structurally dissimilar phases. In addition, switching between the normal and superionic states can take place just within few picoseconds.[93] Consequently, refrigeration cycles based on type-II FICs in principle could be performed at high repetition rates and with no appreciable degradation in cooling performance. On the other hand, mechanical fatigue issues are likely to appear in FICs due to the large changes in volume associated with the normal to superionic phase transition,[89] which may facilitate the nucleation and propagation of cracks and other defects.

D. Organometal halide perovskites

Organometal halide perovskites (OMHPs) are at the frontier of renewable energy research because of their record speed of increasing photovoltaic efficiency and low economical costs associated with their synthesis.[94] The prototypical OMHP is methylammonium lead iodide with the chemical formula $CH_3NH_3PbI_3$. OMHPs present a perovskite structure ABX_3, analogous to that of many ferroelectric oxides, with an organic monovalent cation MA^+ at position A, a divalent metal at position B, and a halide anion at position X. The molecular cation has a permanent dipole and interacts with the inorganic BX_3 motifs through hydrogen bonding and van der Waals interactions.[95] A special feature of OMHPs is that even at room temperature the A-site organic molecules can be orientationally disordered due to their small rotational energy barrier. Such molecular rotations preclude the appearance of long-range ferroelectric order[96] although switchable polar domains have been observed in a number of atomic force microscopy experiments.[97] It is likely then that OMHPs, in analogy to ferroelectric relaxors, are spontaneously polarized at the nanoscale whereas they are polar-compensated at the macroscale. Interestingly, OMHPs are good ionic conductors as well.[98]

OMHPs are mechanically soft as compared to oxide perovskites and can be stretched and compressed significantly even with moderate stresses. Recently, the room-temperature eC response of $CH_3NH_3PbI_3$ has been investigated in detail with simulation methods.[73] A giant adiabatic temperature change of 10.7 K has been predicted to occur for a moderate tensile uniaxial stress of 550 MPa (Table II). The physical origins of such a giant eC effect is the σ-induced frustration of orientational disorder, that is, molecular rotations tend to cease under increasing σ. Specifically, the MA^+ cations are prone to align with the direction of the applied uniaxial stress, thus limiting their rotation, which considerably reduces the entropy of the crystal. It should be noted, however, that the likely effects of ionic transport (i.e., iodine

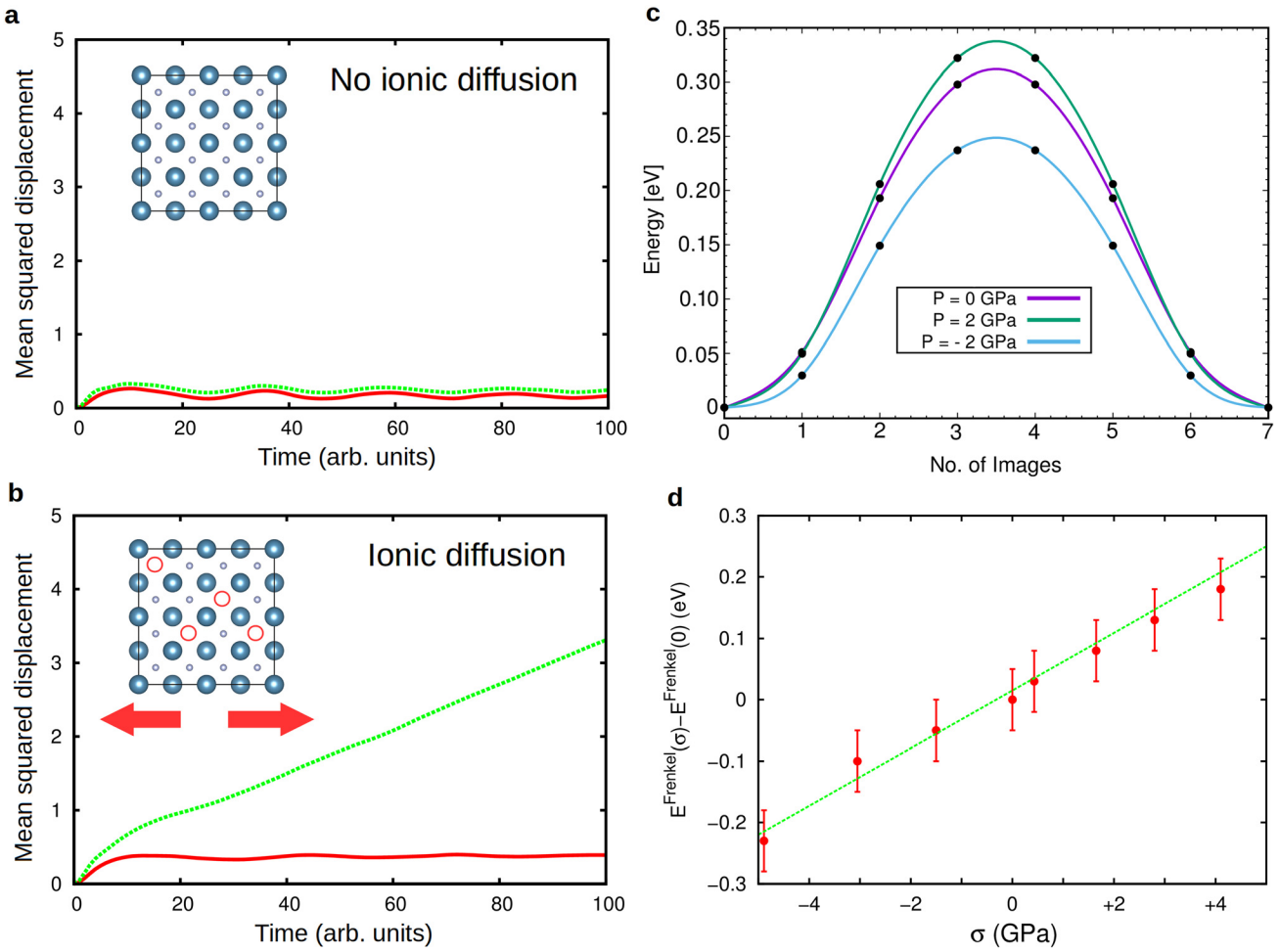

FIG. 6. Representation of the ionic-conductivity enhancement effect driven by mechanical stress in fast-ion conductors. (a) A FIC is in the normal crystalline state. (b) Application of tensile stress stabilizes the superionic state without the need of increasing the temperature. The σ-induced ionic conductivity enhancement effect is originated by the lowering of (c) kinetic energy barriers involved in ionic diffusion and (d) formation energy of Frenkel pair defects. Conversely, compressive stresses tend to deplete ionic conductivity.

vacancies and interstitials diffusion) on the eC response of $CH_3NH_3PbI_3$ have been neglected in work[73] and that in practice those might counteract the adiabatic temperature shift resulting exclusively from the MA^+ degrees of freedom (i.e., eC effects stemming from ionic transport changes are likely to be inverse for uniaxial tensile loads[70,72]). Direct or quasidirect caloric measurements on OMHPs, therefore, are highly desirable for unraveling their real eC potential. Nevertheless, as we explain later on in Sec. V, giant barocaloric effects have been already measured in OMHP near room temperature,[99,100] which reassures the great promise of OMHPs as a novel family of caloric materials.

E. Multiferroics

Multiferroics are materials in which several order parameters coexist, for example, ferroelectricity and magnetism, and can influence each other (that is, are coupled, Fig. 7). Multiferroics have been traditionally investigated in the context of electronic and logic devices and sensors and antennas,[101–103] and as we explain next they also offer interesting possibilities as caloric materials.[104–106] First, in multiferroics different types of external fields can produce different caloric responses and this quality can be exploited to reduce noticeably detrimental hysteresis effects affecting solid-state refrigeration cycles.[46] Second, if the coupling between different order parameters is strong enough, one sole type of external stimulus can produce multiple caloric effects simultaneously, thus potentially enhancing the overall refrigerant performance. For these reasons, multiferroic materials can be also termed as multicaloric. Several theoretical works have focused on establishing the thermodynamics of multicaloric effects[107–109] and in what follows we review their fundamentals.

Let us consider a multiferroic displaying n different types of ferroic orders $\{X_i\}$ $(i = 1, \ldots, n)$ like polarization, magnetization, and lattice strain. For each ferroic property, there is a ferroic field, $\{y_i\}$, that allows to change its value, like electric field, magnetic field, and stress, and therefore to perform some work on the system. In multiferroics, the susceptibility tensor is defined as

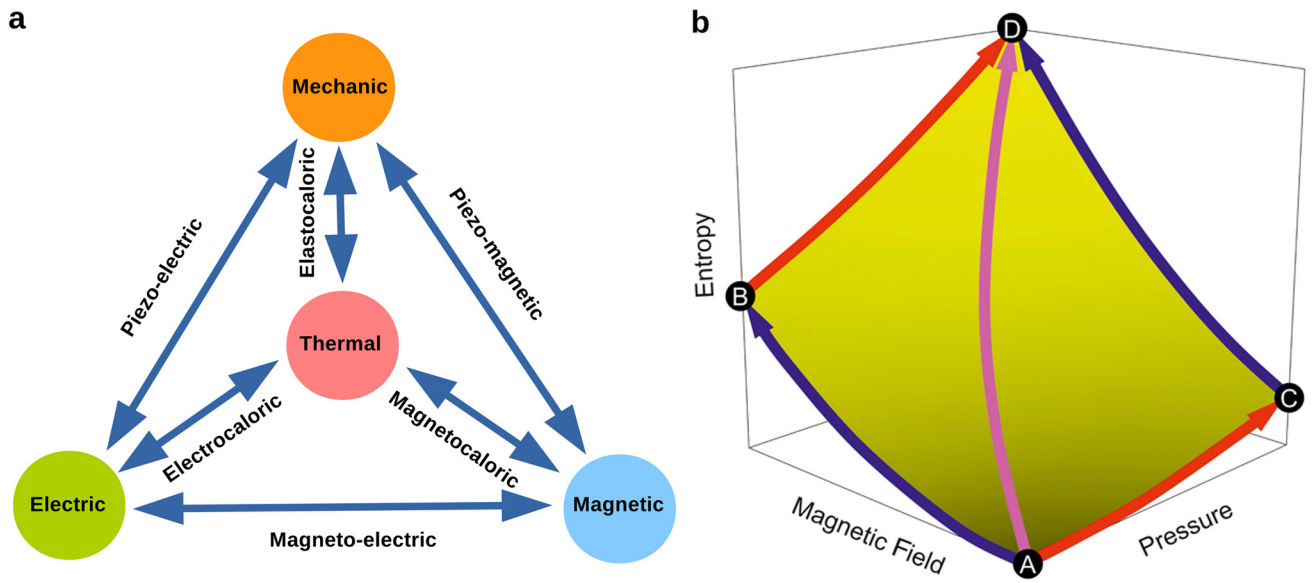

FIG. 7. Multiferroic materials and multicaloric effects. (a) Schematic diagram showing the possible mechanical, electrical, and magnetic couplings in multiferroic materials. The coupling between different order parameters allows for multiple responses of the material upon application of a sole external field, thus producing multiple caloric effects. (b) Schematic variation of isothermal entropy with pressure and magnetic field in a multiferroic material presenting coupling among lattice strain and magnetic order; multicaloric entropy changes can be obtained by applying pressure and magnetic field either sequentially or simultaneously. Reproduced with permission from Stern-Taulats *et al.*, MRS Bull. **43**, 295–299 (2018). Copyright 2018 Materials Research Society.

$$\chi_{ij} = \left(\frac{\partial X_i}{\partial y_j}\right)_{T,\{y_k \neq j\}}, \tag{14}$$

where the diagonal terms correspond to the standard susceptibilities and the cross-coefficients quantify the interplay between different ferroic orders. Multicaloric effects occur when multiple fields are applied either sequentially or simultaneously on a multiferroic material. In the case that the cross-coefficients χ_{ij}'s are large, multicaloric effects also can occur under the action of one sole field.[108]

Let us examine a multiferroic in which two ferroic orders exist, X_1 and X_2, and are strongly coupled (i.e., $\chi_{12} \neq 0$). The isothermal entropy change, ΔS, that results from applying the two external fields y_1 and y_2 on the multicaloric material, either simultaneously or sequentially, is[108,109]

$$\begin{aligned}\Delta S\left[T,\,(0,0) \rightarrow (y_1,y_2)\right] &= \Delta S\left[T,\,(0) \rightarrow (y_1)\right] + \Delta S\left[T,\,(0) \rightarrow (y_2)\right] \\ &+ \int_0^{y_1}\int_0^{y_2}\left(\frac{\partial \chi_{12}}{\partial T}\right) dy_2 dy_1,\end{aligned} \tag{15}$$

where the first two terms on the right-hand side correspond to the usual caloric effects associated with the thermodynamic conjugate variables $\{X_i, y_i\}$ separately (i.e., mechanocaloric, electrocaloric, and magnetocaloric, depending on the nature of the applied external field and material). Likewise, the isothermal entropy change that results from applying one sole type of external field, let us say, y_2, on the same multiferroic compound can be expressed as[108]

$$\Delta S\left[T,\,(0,0) \rightarrow (0,y_2)\right] = \int_0^{y_2}\left[\left(\frac{\partial X_2}{\partial T}\right) + \frac{\chi_{12}}{\chi_{11}} \cdot \left(\frac{\partial X_1}{\partial T}\right)\right] dy_2. \tag{16}$$

To fix ideas, let us consider the explicit case of a mechanocaloric compound that is also ferroelectric (i.e., presents spontaneous and switchable electric polarization). In that particular case, the adiabatic temperature change that follows from applying a mechanical stress, according to Eqs. (9) and (16), can be expressed analytically as

$$\Delta T = -\frac{T}{C} \cdot \int_0^{\sigma}\left[V_0\left(\frac{\partial \varepsilon}{\partial T}\right) + \frac{d_e}{\chi_e}\left(\frac{\partial P}{\partial T}\right)\right] d\sigma, \tag{17}$$

where P represents the electric polarization, d_e is the piezoelectric coefficient ($\partial P/\partial \sigma$), and χ_e is the electric susceptibility ($\partial P/\partial E$, where E represents electric field).

The third and second terms in Eqs. (15) and (16), respectively, offer the possibility of increasing in absolute value the isothermal entropy change, and therefore ΔT, associated with the caloric responses. This is the case, for instance, of the giant multicaloric effects reported for the ferroelectric and antiferroelectric oxide perovskites $PbTiO_3$ (PTO)[79] and $PbZrO_3$,[80] namely, $|\Delta T| \sim 35$ and 25 K, respectively (at operating temperatures of 700 and 950 K), in which strong couplings between lattice strain and the electric polarization exist. We should note, however, that in some cases the primary and secondary caloric effects, that is, those associated with the pairs of thermodynamic variables $\{X_i, y_i\}$ and $\{X_i, y_{j\neq i}\}$, respectively, may have opposite signs and, therefore, lead to the overall reduced caloric activity.[110] For instance, if the multicaloric material described by Eq. (17) is close to a

ferroelectric-paraelectric phase transition, in which $|\partial P/\partial T|$ typically is largest but $\partial P/\partial T < 0$, it is likely that the accompanying ΔT will be reduced as compared to those in analogous nonmultiferroic materials since $\partial\varepsilon/\partial T$ and the coefficients d_e and χ_e normally are positive.

Other areas in which multiferroic materials hold great promise are related to the possibility of improving the degree of reversibility associated with caloric responses by exploiting thermal hysteresis, which in principle is considered as adverse, in beneficial ways. As explained earlier in Sec. III, the degree of reversibility accompanying a caloric process is determined by the hysteresis associated with the underlying phase transition and the fraction of material that undergoes the transition both during cooling and subsequent heating in the cycle. Under the action of multiple external stimulus, the working temperature window associated with the caloric effect can be broadened so that the overlap between the succeeding cooling and heating processes can be increased and the reversibility of the transformations can be enhanced.[111,112]

Meanwhile, hysteresis in multiferroics can be exploited to reduce considerably the intensity of (or time of exposure to) a specific external field in a multiple stimulus cycle. This is the case of $Ni_{49.6}Mn_{35.6}In_{14.8}$ Heusler alloys[46] and FeRh/$BaTiO_3$ heterostructures[113] in which it has been shown that the magnitude of the employed magnetic and electric fields, respectively, can be decreased significantly by combining them with mechanical stresses (Table II). In the case of a ferroelectric compound presenting large piezoelectric coefficients, for instance, in principle it is possible to use compressive stress to make the polarization disappear (that is, to induce the ferroelectric-paraelectric phase transition) while using the electric field to recover the polarization by reverting the transition from the paraelectric to ferroelectric phase; in such a situation even modest electric fields may induce giant caloric effects.[114]

V. BAROCALORIC MATERIALS

Barocaloric (BC) effects are driven by hydrostatic pressure, P. The analytical expression of the accompanying isothermal entropy changes, which is analogous to that of eC effects [Eq. (8)], is

$$\Delta S = -\int_0^P \left(\frac{\partial V}{\partial T}\right)_{P'} dP', \tag{18}$$

where V represents the volume of the system. Large BC effects, therefore, typically occur near first-order transformations that render sizable volume changes. Next, we briefly review the family of materials in which giant barocaloric effects (that is, $|\Delta T| \sim 10$ K and $|\Delta T| \sim 100$ J kg^{-1} K^{-1}) have been discovered. We also highlight recent works in which unconventional barocaloric mechanisms, leading to significant caloric responses, have been reported.

A. Overview of barocaloric performances

In Table III, we enclose some of the most representative BC compounds along with some of their basic refrigerant features. To date, giant BC effects have been experimentally measured in a number of organic-inorganic hybrid perovskites,[99,100] shape-memory alloys,[115–117] polar compounds,[118,119] the archetypal fast-ion conductor AgI,[120] fluoride-based materials,[121] polymers,[122] and molecular crystals.[123–126] The phase transitions leading to the giant BC effects reported in Table III present some similarities to those explained in Secs. III and IV, made the exception of molecular crystals. For instance, for a small hydrostatic pressure (∼100 MPa), the two shape memory alloys $Ni_{51}Mn_{33}In_{16}$ and $Fe_{49}Rh_{51}$ undergo magnetostructural transformations, the two ferroelectric materials $BaTiO_3$ and $(NH_4)_2SO_4$ polar to nonpolar phase transitions, and the rest of compounds purely structural transformations.

Arguably, the less good BC performer is the oxide perovskite $BaTiO_3$ (e.g., low barocaloric strength $|\Delta T|/\Delta P$ and high operating temperature) which only experiences a small relative change in volume of 0.11% during the tetragonal to cubic phase transition[118] (see Sec. IV B). On the other hand, quite remarkable results are the barocaloric strengths and giant adiabatic temperature changes measured in the hybrid perovskite [TPrA][Mn(dca)$_3$] and the fast-ion conductor AgI, respectively (Table III). In the latter system, a record refrigerant cooling performance (RCP, see Sec. II A) of 2.5 kJ kg^{-1} has been measured for $P = 250$ MPa, which results from the existence of large BC effects over an ample temperature span of ∼60 K.[120]

The adiabatic temperature changes measured with quasidirect methods in BC materials are slightly smaller, although comparable in magnitude, than those measured with direct methods in eC materials (i.e., quantities $|\Delta T_{(qd)}|$ and $|\Delta T_{(d)}|$ in Tables III and I, respectively). We note that when comparing different caloric effects in different

TABLE III. Materials in which giant BC effects have been observed experimentally. T_t represents operating temperature, ΔP applied hydrostatic pressure, ΔS_t entropy change associated with the phase transition, and $\Delta T_{(qd)}$ adiabatic temperature change measured with quasidirect methods. "SMA," FE, HP, FIC, and "MC" stand for shape-memory alloys, ferroelectrics, hybrid perovskites, fast-ion conductors, and molecular crystals, respectively. $|\Delta T|/\Delta P$ represents the barocaloric material strength, which is a good indicator of refrigerant performance.

Compound	Material type	T_t (K)	ΔP (MPa)	$\lvert\Delta S_t\rvert$ (J kg^{-1} K^{-1})	$\lvert\Delta T_{(qd)}\rvert$ (K)	$\lvert\Delta T\rvert/\Delta P$ (K MPa^{-1})	References
$Ni_{51}Mn_{33}In_{16}$	SMA	330	250	41	4	0.02	115
$Fe_{49}Rh_{51}$	SMA	310	110	12.5	9	0.08	116, 117
$BaTiO_3$	FE	400	100	2.4	1	0.01	118
$(NH_4)_2SO_4$	FE	220	100	130	8	0.08	119
[TPrA][Mn(dca)$_3$]	HP	330	7	35	5	0.71	99, 100
AgI	FIC	390	250	62	18	0.07	120
$(CH_3)_2C(CH_2OH)_2$	MC	320	520	510	45	0.09	123, 124
$[Fe(pzt)_6](PF_6)_2$	MC	100	100	46	30	0.3	125
$[FeL_2][BF_4]_2$	MC	262	30	80	3	0.1	126

materials one needs to pay special attention to how the experimental data have been determined. For instance, the adiabatic temperature changes that are estimated straightforwardly from the entropy changes associated with the phase transitions normally are much higher than those measured with direct or quasidirect methods (e.g., compare the $|\Delta T_t|$ and $|\Delta T_{(q)}|$ values in Table I).

In BC materials, the discrepancies between $|\Delta T_t|$ and $|\Delta T_{(qd)}|$ can be particularly large (e.g., they amount to ∼30 K in $Ni_{51}Mn_{33}In_{16}$[10]) due to two main causes. First, the lack of adiabaticity associated with the pressure transmitting medium which may not be perfectly isotropic. And second, the partial completion of the involved phase transition owing to phase coexistence and hysteresis effects that typically accompany first-order transformations. Such adverse effects, which may lead to limiting irreversibility issues, in principle are not so critical in eC materials since pressure transmitting media are not required and the involved phase transitions can be driven to completion more efficiently. An illustrative example of this aspect is the eC effects observed in Ni-Ti alloys, which are one of the largest reported to date and for which the differences between $|\Delta T_t|$ and $|\Delta T_{(d)}|$ are practically negligible (Table I).[10]

B. Recent developments

The barocaloric strengths and giant adiabatic temperature changes experimentally measured in molecular crystals, which have been reported within the last few years, are very impressive. For instance, the $|\Delta T_{(qd)}|$ obtained in neopentylglycol, with the chemical formula $(CH_3)_2C(CH_2OH)_2$,[1,123,124] amounts to 45–50 K near room temperature, which actually deserves the adjective "colossal." On the other hand, the $\Delta T/\Delta P$ values reported for the magnetic compounds $[Fe(pzt)_6](PF_6)_2$[125] and $[FeL_2][BF_4]_2$[126] are superior to those achieved in the rest materials listed in Table III, made the exception of the hybrid perovskites $[TPrA][Mn(dca)_3]$ (although their corresponding operating temperatures are probably too low). Next, we explain in more detail the atomistic mechanisms leading to such large and promising caloric effects observed in molecular crystals.

Plastic crystals are molecular solids in which the interactions between molecules are very weak and long-ranged (that is, dispersion like). As a consequence, plastic crystals are highly compressible and can be deformed in a reversible manner, hence the adjective "plastic." Under certain pressure and temperature conditions, molecules in plastic crystals can start rotating almost freely around their centers of mass. The centers of mass remain localized at well-defined and ordered positions in the crystal lattice, while molecular rotation leads to orientational disorder characterized by high entropy. By means of external pressure, it is possible to block such molecules rotations, thus inducing a fully ordered state with lower entropy.

Very recently, it has been shown by several independent research groups[123,124] that the entropy changes driven by pressure near 300 K in plastic crystals are huge and render colossal BC effects [see $(CH_3)_2C(CH_2OH)_2$ in Table III]. It is worth mentioning that similar σ-induced caloric mechanisms were predicted previously in $CH_3NH_3PbI_3$ based on the outcomes of classical molecular dynamics simulations[73] (Sec. IV D). In view of the high anharmonicity and mechanical softness of plastic crystals, and of the results reported previously for organometal halide perovskites,[73] it is very likely that analogous caloric responses induced by uniaxial stresses, leading to huge eC effects, could be achieved in practice (provided that the samples are not brittle). Figure 8 sketches a possible 4-step cooling cycle based on the colossal BC effects disclosed in plastic crystals.

Plastic crystals are quite different from other caloric materials, not just because of their huge entropy changes near room temperature: they are cheap and easy to produce, lightweight, nontoxic, and some of them are flexible. Plastic crystals, therefore, seem to be specifically well suited for the integration of solid-state cooling in electronic devices and portable applications. Nevertheless, plastic crystals also suffer from some important problems in the context caloric materials.

For instance, given their organic nature, plastic crystals have relatively low melting points [typically about 300–400 K (Ref. 127)] which is not desirable for refrigeration applications. Likewise, the heat conductivity of plastic crystals typically is very low [on the order of ∼0.1 W mK^{-1} (Ref. 132)], thus making the transport of heat in hypothetical solid-state cooling devices difficult. In addition, the fact that most plastic crystals are highly deformable suggests that these materials probably lack the necessary mechanical resilience for enduring a large number of refrigeration cycles. Last but not least, hysteresis and phase-coexistence effects are likely to weaken the cooling performance of some plastic crystals due to the first-order nature of the molecular order-disorder phase transformation. A possible solution to address this latter technical issue may consist in combining multiple external stimulus, as explained in Sec. IV E, like electric fields and mechanical stresses (that is, molecules in plastic crystals may present an electric dipole and thus react to external electric bias).

Recently, large BC effects have been first predicted and subsequently demonstrated experimentally in magnetic materials undergoing spin-crossover (SCO) phase transitions. Spin-crossover phase transitions refer to transformations from a low-spin state to a high-spin state as induced by increasing temperature, which typically are accompanied by large volume changes and may occur near or beyond room temperature.[128] By applying and removing hydrostatic pressure on SCO compounds (typically ∼0.01–0.1 GPa), it is also possible to trigger the transition from low-spin to high-spin state and vice versa. Archetypal SCO materials are molecular crystals that contain magnetic transition metal ions (e.g., Fe),[125,126] and the usual order of magnitude of the entropy changes associated with their transformations is ∼100 J kg^{-1} K^{-1}.[128]

The origins of the large entropy changes found in SCO materials are linked to both magnetic spin ordering and lattice vibrations, which are very likely to be strongly coupled.[105] However, design strategies able to optimize both entropy increments systematically have not emerged yet presumably due to the lack of related theoretical studies based on first-principles methods (in which the magnetic spin and lattice degrees of freedom in principle can be described accurately and on an equal footing[39,105]). A potential benefit of SCO compounds is that they are highly tuneable in the sense that by changing some of their molecular building motifs the critical temperature and volume change accompanying the spin-state transition can be modified appreciably.[128,129]

VI. CONCLUDING REMARKS AND OUTLOOK

Solid-state cooling is an environmentally friendly, energy-efficient, and highly scalable technology that may solve most of the problems associated with current refrigeration methods based on gas compression-decompression cycles (including, potential toxicity and green-house effects). It relies on applying external magnetic, electric,

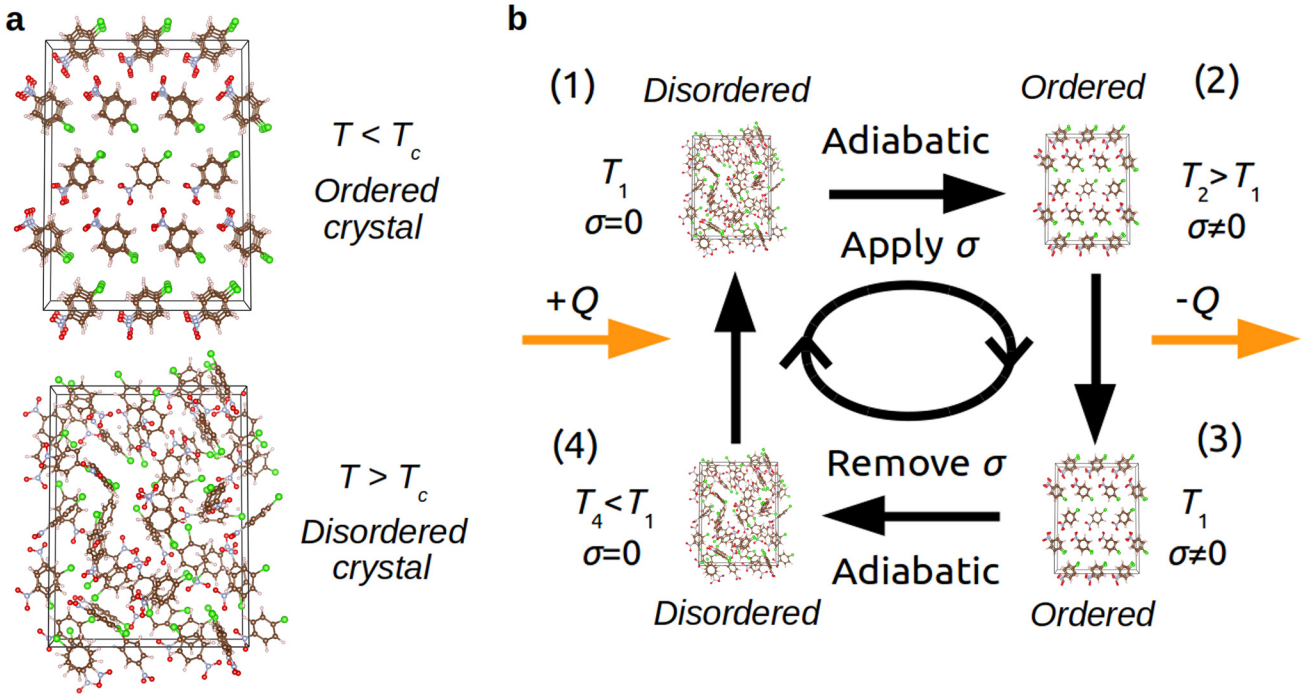

FIG. 8. The molecular order-disorder phase transition in plastic crystals and their potential use in solid-state cooling. (a) The molecular ordered and disordered phases of a plastic crystal are sketched; the disordered high-entropy phase is stabilized at high temperatures while the ordered low-entropy phase is stabilized at low temperatures. (b) Proposal of a simple four-step refrigeration cycle based on external pressure, σ, and plastic crystals; (1) initially the crystal is in the molecular disordered phase; (2) pressure is applied adiabatically on the crystal so that the ordered phase is stabilized and the temperature of the crystal increases; (3) heat is ejected from the system and the temperature of the crystal returns to its initial value; (4) pressure is released adiabatically from the crystal so that the disordered phase is recovered and the temperature of the crystal decreases; the cycle is completed by absorbing the heat from a hot source and returning to the initial temperature.

mechanical fields, or a combination of them, on compounds that undergo temperature variations as a result of field-induced phase transitions that involve large changes in entropy. Mechanocaloric effects, either produced by uniaxial stress or hydrostatic pressure, render the largest adiabatic temperature variations of all caloric responses, typically $\Delta T \sim 10$ K; hence, they are particularly promising from an applied perspective.

Elastocaloric effects probably are the most encouraging when it comes to practical applications. Since they do not require a pressure-transmitting medium, the involved phase transitions can be driven to completion more easily, and both compressive and tensile stress can be applied; hence, *a priori* richer caloric responses can be attained (in contrast to hydrostatic pressure, which in practice only can be compressive). Furthermore, most mechanocaloric compounds do not suffer from limiting issues caused by the application of external fields (e.g., leakage currents and dielectric losses in electrocaloric materials) and are relatively abundant in nature (in contrast, for instance, to prototype magnetocaloric materials which contain rare-earth elements).

In the present review, we have explained the key properties of archetypal and nonconventional families of mechanocaloric materials (e.g., NiTi-based shape memory alloys and superionic compounds, respectively). Although conventional mechanocaloric materials already display superb cooling performances (e.g., $\Delta T = 25$ K near room temperature upon the application-removal of ~500 MPa uniaxial tensile stress in Ni-Ti wires[43,44]), they are not perfect and present also few important drawbacks. Such limitations are mainly related to hysteresis and materials' fatigue issues leading to irreversibility and poor cyclability, which may compromise seriously the performance of refrigeration cycles in practice. Nevertheless, a number of new mechanocaloric materials and ingenious multiple stimulus strategies have been proposed recently that can potentially overcome those problems and thus advance the field of solid-state cooling.

On the materials side, it is possible to find mechanocaloric compounds exhibiting second-order, or weak first-order, phase transitions which by definition entail small hysteresis and can somehow be triggered reversibly. Examples of such materials include inorganic ferroelectrics (e.g., oxide perovskites) and type-II fast-ion conductors (e.g., PbF_2 and Li_3N). In the particular case of type-II fast-ion conductors, mechanocaloric effects are originated by order-disorder phase transitions affecting the sublattice of mobile ions as the material enters the superionic state. Nevertheless, the operating temperatures associated with some ferroelectrics and fast-ion conductors normally are well above or below room temperature, which suggests the use of additional doping strategies in order to shift the corresponding transition temperatures.

Meanwhile, colossal mechanocaloric effects [$\Delta T \sim 50$ K near room temperature for relatively small hydrostatic pressures of ~0.5 GPa (Refs. 123 and 124)] have been discovered very recently in a class of molecular solids known as plastic crystals (e.g., neopentylglycol), which are also related to pressure-driven order-disorder phase

transitions (it remains to be demonstrated whether analogous elastocaloric effects also exist in such materials). Interestingly, other types of molecular solids like organic-inorganic hybrid perovskites and spin-crossover (SCO) complexes have been reported to exhibit giant mechanocaloric effects as well in the last few years. In view of the colossal mechanocaloric effects measured in molecular and disordered crystals and of their fresh appearance in the context of caloric effects, there seems to be a lot of room for advancements based on them in the near future.

On the multiple external stimulus side, it has been also shown recently that the combination of multiple external fields, applied either sequentially or simultaneously, on multiferroic materials (typically, magnetic Heusler alloys and oxide perovskites) may be very advantageous in terms of enhanced reversibility, enhanced caloric response, and reduction in the intensity of the applied coercive fields (this last point turns out to be especially relevant for magnetocaloric materials[46,113]). For these multiple external field approaches to succeed, it is crucial to find suitable multiferroic materials in which several order parameters coexist and (ideally) are strongly coupled. In customary multiferroic compounds, lattice strain appears most of the times intertwined with the polar or magnetic degrees of freedom; hence, one of the multiple external fields should preferably be mechanical stress (leading to combined electric field-mechanical stress or magnetic field-mechanical stress cycles). Research on multicaloric effects and multicaloric cycles is in its early stage, and there seems to be also a lot of promise along those directions.

The present review on nonconventional mechanocaloric materials and mechanocaloric effects aims to motivate new theoretical and experimental research on solid-state cooling. Our critical assessment of materials suggests that solid-state cooling technologies could benefit immensely from the intensive research already undertaken in highly active research fields including functional materials (multiferroic, ferroelectric, and magnetic compounds), energy storage (fast-ion conductors), and coordination chemistry (plastic and molecular crystals).

REFERENCES

[1]C. Cazorla, Nature **567**, 470 (2019).
[2]See http://www.iifiir.org/userfiles/file/publications/notes/NoteTech_35_EN_uz7bwths.pdf for a report on refrigeration data from the International Institute of Refrigeration.
[3]C. B. Zimm, A. Jastrab, A. Sternberg, V. Pecharsky, K. Gschneidner, M. Osborne, and I. Anderson, Adv. Cryog. Eng. **43**, 1759 (1998).
[4]K. A. Gschneidner, V. K. Pecharsky, and A. O. Tsokol, Rep. Prog. Phys. **68**, 1479 (2005).
[5]A. S. Mischenko, Q. Zhang, J. F. Scott, R. W. Whatmore, and N. D. Mathur, Science **311**, 1270 (2006).
[6]J. F. Scott, Annu. Rev. Mater. Res. **41**, 229 (2011).
[7]H. Wang, L. Zhang, Y. Sun *et al.*, Scr. Mater. **178**, 150 (2020).
[8]See https://energy.gov/eere/buildings/downloads/non-vapor-compression-hvac-technologies-report for "Energy Savings Potential and RD&D Opportunities for Non-Vapor-Compression HVAC Technologies, Report of the U.S. Dept. of Energy" (last accessed March, 2014).
[9]J. Tusek *et al.*, Acta Mater. **150**, 295 (2018).
[10]L. Mañosa and A. Planes, Adv. Mater. **29**, 1603607 (2017).
[11]L. Mañosa and A. Planes, Philos. Trans. R. Soc. A **374**, 20150310 (2016).
[12]J. Tusek, K. Engelbrecht, L. Mañosa, E. Vives, and N. Pryds, Shape Mem. Superelasticity **2**, 317 (2016).
[13]B. Lu and J. Liu, Sci. Bull. **60**, 1638 (2015).
[14]V. K. Pecharsky and K. A. Gschneidner, Jr., Phys. Rev. Lett. **78**, 4494 (1997).
[15]C. Rodriguez and L. C. Brown, Metall. Mater. Trans. A **11**, 147 (1980).
[16]K. Mukherjee, S. Sircar, and N. B. Dahotre, Mater. Sci. Eng. **74**, 75 (1985).
[17]E. Bonnot *et al.*, Phys. Rev. Lett. **100**, 125901 (2008).
[18]X. Moya, E. Defay, V. Heine, and N. D. Mathur, Nat. Phys. **11**, 202 (2015).
[19]F. Cheng, L. Gao, Y. Wang, J. Wang, X. Liao, and S. Yang, J. Magn. Magn. Mater. **478**, 234 (2019).
[20]S. Qian, Y. Geng, Y. Wang *et al.*, Int. J. Refrig. **64**, 1 (2016).
[21]S. Qian, Y. Wu, J. Ling, J. Muehlbauer, Y. Hwang, I. Takeuchi, and R. Radermacher, in Proceedings of the International Congress on Refrigeration, IIF-IIR, Yokohama Japan (2015), p. 92.
[22]S. Qian, Y. Geng, Y. Wang, J. Muehlbauer, J. Ling, Y. Hwang, R. Radermacher, and I. Takeuchi, Sci. Technol. Built Environ. **22**, 500 (2016).
[23]H. Ossmer, C. Chluba, S. Kaufmann-Weiss, E. Quandt, and M. Kohl, APL Mater. **4**, 064102 (2016).
[24]J. Tusek, K. Engelbrecht, R. Millan-Solsona, L. Manosa, E. Vives, L. P. Mikkelsen, and N. Pryds, Adv. Energy Mater. **5**, 1500361 (2015).
[25]J. Tusek, K. Engelbrecht, D. Eriksen, S. Dall'Olio, J. Tusek, and N. Pryds, Nat. Energy **1**, 16134 (2016).
[26]X. Moya, S. Kar-Narayan, and N. D. Mathur, Nat. Mater. **13**, 439 (2014).
[27]D. S. Kim, B. C. Kim, S. H. Han *et al.*, J. Appl. Phys. **126**, 234101 (2019).
[28]C. Cazorla and J. Boronat, Rev. Mod. Phys. **89**, 035003 (2017).
[29]C. Cazorla, Coord. Chem. Rev. **300**, 142 (2015).
[30]S. Lisenkov, R. Herching, S. Patel, R. Vaish, J. Cuozzo, and I. Ponomareva, Nano Lett. **16**, 7008 (2016).
[31]S. Lisenkov and I. Ponomareva, Phys. Rev. B **86**, 104103 (2012).
[32]S. Baroni, P. Giannozzi, and E. Isaev, Rev. Mineral. Geochem. **71**, 39 (2010).
[33]C. Cazorla and T. Gould, Sci. Adv. **5**, eaau5832 (2019).
[34]D. Alfe, Comput. Phys. Commun. **180**, 2622 (2009).
[35]A. Togo and I. Tanaka, Scr. Mater. **108**, 1 (2015).
[36]C. Cazorla and D. Errandonea, Phys. Rev. B **98**, 186101 (2018).
[37]J. Klarbring and S. I. Simak, Phys. Rev. Lett. **121**, 225702 (2018).
[38]A. K. Sagotra, D. Chu, and C. Cazorla, Phys. Rev. Mater. **3**, 035405 (2019).
[39]C. Cazorla, O. Dieguez, and J. Iniguez, Sci. Adv. **3**, e1700288 (2017).
[40]N. A. Zarkevich, D. D. Johnson, and V. K. Pecharsky, J. Phys. D **51**, 024002 (2018).
[41]J. D. Bocarsly, E. E. Levin, C. A. C. Garcia, K. Schwennicke, S. D. Wilson, and R. Seshadri, Chem. Mater. **29**(4), 1613 (2017).
[42]A. Planes and L. Mañosa, Solid State Phys. **55**, 159 (2001).
[43]J. Cui, Y. Wu, J. Muehlbauer *et al.*, Apply. Phys. Lett. **101**, 073904 (2012).
[44]J. Tusek, K. Engelbrecht, L. P. Mikkelsen, and N. Pryds, J. Apply. Phys. **117**, 124901 (2015).
[45]H. Ossmer, F. Lambrecht, M. Gultig *et al.*, Acta Mater. **81**, 9 (2014).
[46]T. Gottschall *et al.*, Nat. Mater. **17**, 929 (2018).
[47]G. J. Pataky, E. Ertekin, and H. Sehitoglu, Acta Mater. **96**, 420 (2015).
[48]C. Chluba, W. Ge, R. Lima de Miranda *et al.*, Science **348**, 1004 (2015).
[49]C. Chluba, H. Ossmer, C. Zamponi *et al.*, Shape Mem. Superelasticity **2**, 95 (2016).
[50]E. Vives, S. Burrows, R. S. Edwards *et al.*, Appl. Phys. Lett. **98**, 011902 (2011).
[51]L. Mañosa, S. Jarque-Farnos, E. Vives, and A. Planes, Appl. Phys. Lett. **103**, 211904 (2013).
[52]S. A. Nikitin, G. Myalikgulyev, M. P. Annaorazov *et al.*, Phys. Lett. A **171**, 234 (1992).
[53]F. Xiao, T. Fukuda, and T. Kakeshita, Appl. Phys. Lett. **102**, 161914 (2013).
[54]M. Schmidt, J. Ullrich, A. Wieczorek *et al.*, Shape Mem. Superelasticity **1**, 132 (2015).
[55]Y. Xu, B. Lu, W. Sun *et al.*, Appl. Phys. Lett. **106**, 201903 (2015).
[56]F. Xiao, M. Jin, and X. Jin, Acta Mater. **96**, 292 (2015).
[57]P. O. Castilla-Villa, L. Mañosa, A. Planes *et al.*, J. Appl. Phys. **113**, 053506 (2013).
[58]R. Millan-Solsona, E. Stern-Taulats, E. Vives *et al.*, Appl. Phys. Lett. **105**, 241901 (2014).
[59]W. Sun, J. Liu, B. Lu *et al.*, Scr. Mater. **114**, 1 (2016).
[60]B. Lu, P. Zhang, Y. Xu *et al.*, Mater. Lett. **148**, 110 (2015).
[61]Y. J. Huang, Q. D. Hu, N. M. Bruno *et al.*, Scr. Mater. **105**, 42 (2015).
[62]Z. Xie, G. Sebald, and D. Guyomar, Appl. Phys. Lett. **107**, 081905 (2015).
[63]Y. Yoshida, K. Yuse, D. Guyomar, J.-F. Capsal, and G. Sebald, Appl. Phys. Lett. **108**, 242904 (2016).
[64]S. Patel, A. Chauhan, R. Vaish, and P. Thomas, Appl. Phys. Lett. **108**, 072903 (2016).

[65]Y. Liu, I. C. Infante, X. Lou *et al.*, Adv. Mater. **26**, 6132 (2014).
[66]Y. Liu, J. Wei, P.-E. Janolin *et al.*, Phys. Rev. B **90**, 104107 (2014).
[67]A. Chauhan, S. Patel, and R. Vaish, Appl. Phys. Lett. **106**, 172901 (2015).
[68]F. Wang, B. Li, Y. Ou *et al.*, Mater. Lett. **206**, 189 (2017).
[69]S. Lisenkov and I. Ponomareva, Phys. Rev. Mater. **2**, 055402 (2018).
[70]C. Cazorla and D. Errandonea, Nano Lett. **16**, 3124 (2016).
[71]A. K. Sagotra, D. Errandonea, and C. Cazorla, Nat. Commun. **8**, 963 (2017).
[72]A. K. Sagotra, D. Chu, and C. Cazorla, Nat. Commun. **9**, 3337 (2018).
[73]S. Liu and R. E. Cohen, J. Phys. Chem. C **120**, 17274 (2016).
[74]J. P. Joule, Philos. Trans. **149**, 91 (1859).
[75]Z. Xie, G. Sebald, and D. Guyomar, Appl. Phys. Lett. **108**, 041901 (2016).
[76]B. Neese, B. Chu, S. G. Lu *et al.*, Science **321**, 821 (2008).
[77]N. M. Bom, W. Imamura, E. O. Usuda, L. S. Paixao, and A. M. G. Carvalho, ACS Macro Lett. **7**, 31 (2018).
[78]A. M. G. Carvalho, W. Imamura, E. O. Usuda, and N. M. Bom, Eur. Polym. J. **99**, 212 (2018).
[79]S. Lisenkov, B. K. Mani, C.-M. Chang, J. Almand, and I. Ponomareva, Phys. Rev. B **87**, 224101 (2013).
[80]S. Lisenkov, B. K. Mani, J. Cuozzo, and I. Ponomareva, Phys. Rev. B **93**, 064108 (2016).
[81]C. Cazorla and M. Stengel, Phys. Rev. B **92**, 214108 (2015).
[82]J. X. Zhang, X. X. Ke, G. Y. Gou *et al.*, Nat. Commun. **4**, 2768 (2013).
[83]W. Zhong and D. Vanderbilt, Phys. Rev. B **53**, 5047 (1996).
[84]K. Gesi, Ferroelectrics **203**, 249 (1997).
[85]F. Cordero, F. Cracium, F. Trequattrini, E. Mercadelli, and C. Galassi, Phys. Rev. B **81**, 144124 (2010).
[86]J. Iniguez and D. Vanderbilt, Phys. Rev. Lett. **89**, 115503 (2002).
[87]H. Meng, B. Li, W. Ren, and Z. Zhang, Phys. Lett. A **377**, 567 (2013).
[88]F. Wang, B. Li, Y. Ou *et al.*, RSC Adv. **6**, 70557 (2016).
[89]S. Hull, Rep. Prog. Phys. **67**, 1233 (2004).
[90]C. Cazorla and D. Errandonea, Phys. Rev. Lett. **113**, 235902 (2014).
[91]C. Cazorla, Res. Phys. **5**, 262 (2015).
[92]A. K. Sagotra and C. Cazorla, ACS Appl. Mater. Interfaces **9**, 38773 (2017).
[93]T. A. Miller, J. S. Wittenberg, H. Wen *et al.*, Nat. Commun. **4**, 1369 (2013).
[94]D. A. Egger, A. Bera, D. Cahen *et al.*, Adv. Mater. **30**, 1800691 (2018).
[95]J. F. Dobson and T. Gould, J. Phys.: Condens. Matter **24**, 073201 (2012).
[96]A. Filippetti, P. Delugas, M. I. Saba, and A. Mattoni, J. Phys. Chem. Lett. **6**, 4909 (2015).
[97]M. Coll, A. Gomez, E. Mas-Marza *et al.*, J. Phys. Chem. Lett. **6**, 1408 (2015).
[98]C. Eams, J. M. Frost, P. R. F. Barnes *et al.*, Nat. Commun. **6**, 7497 (2015).
[99]J. M. Bermudez-Garcia, M. Sanchez-Andujar, S. Castro-Garcia *et al.*, Nat. Commun. **8**, 15715 (2017).
[100]J. M. Bermudez-Garcia, M. Sanchez-Andujar, and M. A. Senaris-Rodriguez, J. Phys. Chem. Lett. **8**, 4419 (2017).
[101]R. Ramesh and N. A. Spaldin, Nat. Mater. **6**, 21 (2007).
[102]N. A. Spaldin and R. Ramesh, Nat. Mater. **18**, 203 (2019).
[103]J. T. Heron *et al.*, Nature **516**, 370 (2014).
[104]A. Planes, T. Castan, and A. Saxena, Philos. Trans. R. Soc. London A **374**, 20150304 (2016).
[105]C. Cazorla and J. Iniguez, Phys. Rev. B **98**, 174105 (2018).
[106]S. Crossley, W. Li, X. Moya, and N. Mathur, Philos. Trans. R. Soc. London A **374**, 20150313 (2016).
[107]M. M. Vopson, J. Phys. D **46**, 345304 (2013).
[108]A. Planes, T. Castan, and A. Saxena, Philos. Mag. **94**, 1893 (2014).
[109]E. Stern-Taulats, T. Castan, L. Manosa *et al.*, MRS. Bull. **43**, 295 (2018).
[110]T. Tong, J. Karthik, R. V. K. Mangalam, L. W. Martin, and D. G. Cahill, Phys. Rev. B **90**, 094116 (2014).
[111]E. Stern-Taulats, T. Castán, A. Planes, L. H. Lewis, R. Barua, S. Pramanick, S. Majumdar, and L. Manosa, Phys. Rev. B **95**, 104424 (2017).
[112]A. Gràcia-Condal, E. Stern-Taulats, A. Planes, and L. Mañosa, Phys. Rev. Mater. **2**, 084413 (2018).
[113]Y. Liu, L. C. Phillips, R. Mattana, M. Bibes, A. Barthelemy, and B. Dkhil, Nat. Commun. **7**, 11614 (2016).
[114]Y. Liu, J. F. Scott, and B. Dkhil, APL Mater. **4**, 064109 (2016).
[115]E. Stern-Taulats, A. Planes, P. Lloveras *et al.*, Acta Mater. **96**, 324 (2015).
[116]E. Stern-Taulats, A. Planes, P. Lloveras *et al.*, Phys. Rev. B **89**, 214105 (2014).
[117]E. Stern-Taulats, A. Gracia-Condal, A. Planes *et al.*, Appl. Phys. Lett. **107**, 152409 (2015).
[118]E. Stern-Taulats, P. Llovera, M. Barrio *et al.*, APL Mater. **4**, 091102 (2016).
[119]P. Lloveras, E. Stern-Taulats, M. Barrio *et al.*, Nat. Commun. **6**, 8801 (2015).
[120]A. Aznar, P. Lloveras, M. Romanini *et al.*, Nat. Commun. **8**, 1851 (2017).
[121]M. Gorev, E. Bogdanov, I. N. Flerov, and N. M. Laptash, J. Phys.: Condens. Matter **22**, 185901 (2010).
[122]E. L. Rodriguez and F. E. Filisko, J. Appl. Phys. **53**, 6536 (1982).
[123]B. Li *et al.*, Nature **567**, 506 (2019).
[124]P. Lloveras *et al.*, Nat. Commun. **10**, 1803 (2019).
[125]P. J. von Ranke, B. P. Alho, and P. O. Ribeiro, J. Alloys Compd. **749**, 556 (2018).
[126]S. P. Vallone *et al.*, Adv. Mater. **31**, 1807334 (2019).
[127]A. Aznar, P. Lloveras, and J. L. Tamarit, Eur. Phys. J.: Spec. Top. **226**, 1017 (2017).
[128]K. G. Sandeman, APL Mater. **4**, 111102 (2016).
[129]P. J. von Ranke, Appl. Phys. Lett. **110**, 181909 (2017).
[130]D. Cong *et al.*, Phys. Rev. Lett. **122**, 255703 (2019).
[131]A. Aznar *et al.*, Adv. Mater. **31**, 1903577 (2019).
[132]A. I. Krivchikov *et al.*, J. Non-Cryst. Solids **407**, 141 (2015).
[133]J. Quarini and A. Prince, Proc.-Inst. Mech. Eng.: J. Mech. Eng. Sci. **218**, 1175 (2004).